Novel System for Zero-Power, Orientation-Controlled Magnetic Levitation

James Lin , Akinori Harada, Koichi Oka

Department of Intelligent Mechanical Systems Engineering, Kochi University of Technology, Tosyamada, Kami City, Kochi, Japan

***Abstract*— A novel system is described for achieving orientation controlled zero power levitation. The principles of operation are explained, as well as the zero power feedback control strategy. Expected system limitations and system parameter selection is discussed. Numerical data is presented in support of the feasibility of the system and controller.**

A. Introduction

The ability to magnetically levitate a rigid body in more than one dimension, with zero power, using fixed hybrid electromagnets (HEMs) is inherently dependent on the orientation of the levitated body, as the attractive force of the permanent magnets are dependent on the air gap between the HEM and the target. Such zero power magnetically levitated platforms will increase the magnitude of their tilt as the eccentricity of the load is increased [1,2].

For many operations, it is desirable to be able to select the orientation of the levitated object. To achieve zero power performance while maintaining a level orientation, a novel system is proposed here. Fig. 1 outlines this system, where the active components are on a fixed stage with a free floating passive platform. Such a configuration would be beneficial in pick and place operations, where the active components would exist on a robotic arm. Alternatively, the active components could exist on the levitated platform with a passive target. Such a configuration could be suited for a 2 dimensional conveyance if combined with an x-y inductive motor, however, due to the non-static nature of the HEM positions, the system would not be suited towards conveyance along a 1 dimensional rail system [1].

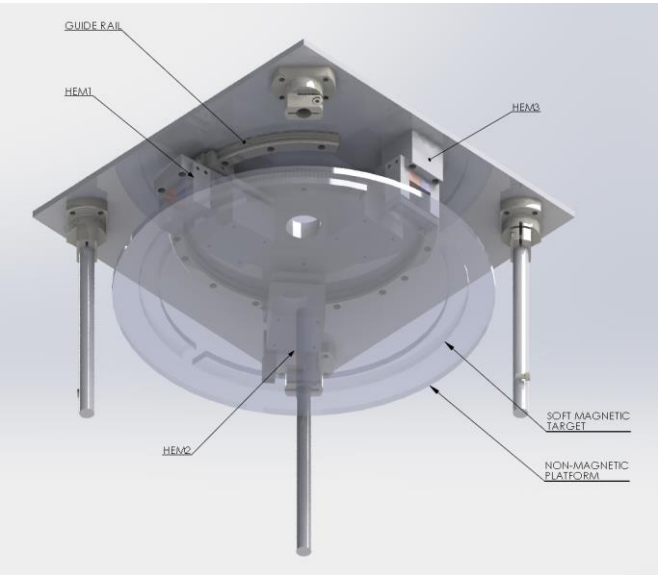

Figure 1. Perspetive view of system where passive platform is suspended below HEM array. Some parts hidden or shown as transparent. HEM3 is fixed, while HEM1 and HEM2 rotate about the guide rails.

B. Hardware

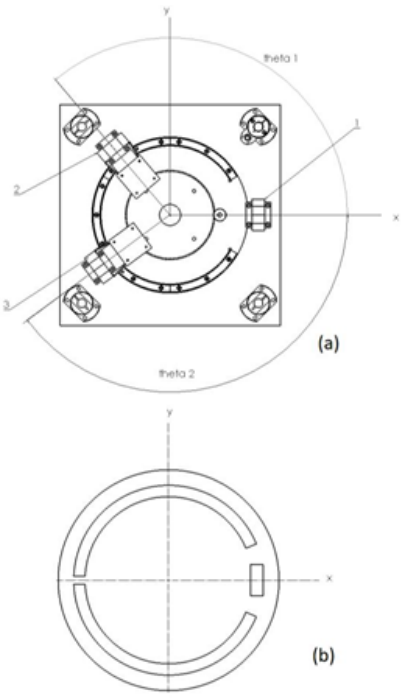

Figure 2. (a) Detiled view of active top layer. Two HEMs rotate around the guide rail at angles θ_1 and θ_2, while the third remains fixed. (b) Passtive platform where only the target strips are magnetically permeable.

The novel design of this system differs from typical zero power levitation paradigms in employing two HEMs which move circularly on a guide rail, driven by the gear system as detailed in fig. 2(a). The passive magnetic target is detailed in fig. 2(b), where its geometry allows for the electrometric circuit at each HEM shown in fig. 3. The third HEM remains fixed, and its small target aids in passively controlling platform rotation about the z-axis. Together, the geometry of all three HEMs and targets aid in the passive control of the platforms lateral motion in x and y.

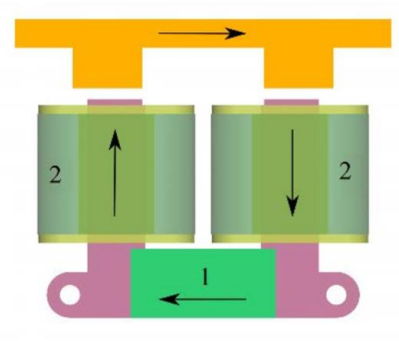

Figure 3. Example of a typical HEM consisting of electromagnetic coils (2) and a permanent magnet (1). The passive target, shown in yellow, allows the completion of the electromagnetic circuit. [1]

C. Operating Space

It is anticipated that the levitated platform will be loaded eccentrically with mass. It is important to consider under what loading conditions zero power levitation can be achieved. For level levitation, the air gap between each HEM and its target must be identical, therefore, the attractive force at each HEM will be equal. Geometrically then, zero power levitation can only be achieved when the overall center of mass is at the centroid of the three HEMs. The x and y values for centroid C in terms of θ_1 and θ_2 is given as:

$$C_{x,y} = \left\{\frac{r}{3}(\cos\theta_1 + \cos\theta_2 + 1), \frac{r}{3}(\sin\theta_1 - \sin\theta_2)\right\} \quad (1)$$

Where r is the distance from the center of rotation to each HEM. An example orientation is visualized in fig. 4.

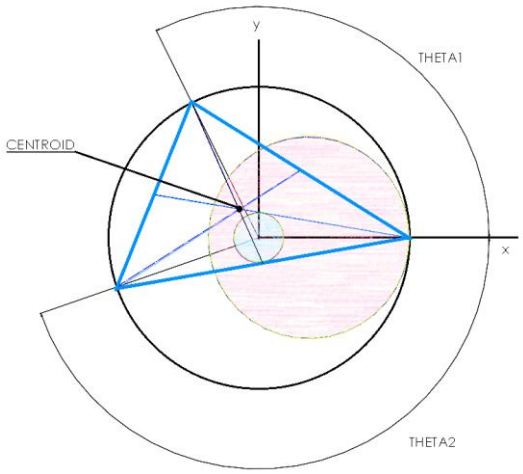

Figure 4. Example centroid of HEMs. Mathematically achievable operating space shaded in pink. Engineering operating space shaded in blue.

All achievable centroid positions achievable by eq. (1) were numerically calculated and are shown as the pink shaded area in fig. 4. The solution is asymmetric due to the single HEM at location three being fixed. Practically, all mathematical solutions cannot be achieved due to the fact that the HEMs physically occupy space and cannot overlap.

Applying the constraints that the HEMs will not be within 15 angular degrees of one another, HEM 1 should not move into the negative y space, HEM 2 should not move into the positive y space, and the operatizing space should be radially symmetric, a final selected operating space in which the overall center of mass of the system should exist was selected and is shaded in blue in fig. 4. Mathematically, this space is a circle of size 0.2r, and is limited by moving the center of mass long the y axis. This engineering operating space aids the assumption that the system rotates about its geometric center, as well as offers operational practicality.

D. Controllability and Observatbility

The controllability and observability of the linearized system at all operating points is validated, where the following terminology is used:

z_0 – z height of center of platform
$i_{0,n}$ – Initial current in HEM 'n'
$\propto$ - Tipping angle
β – Tilting angle
$F_{z,n}$ – Force contribution at HEM 'n' from initial height
$F_{i,n}$ – Force contribution at HEM 'n' from initial current
F_n – Force at HEM 'n'
δz – Small height displacement of platform center
k_{i} – Current stiffness matrix
k_z – Air gap stiffness matrix
F_z – Equivalent force at center of platform
T_x – Equivalent moment around x
$\mathrm{T_y}$ – Equivalent moment about y
F_n – Total force at HEM 'n'

A simplified schematic is shown in fig. 5.

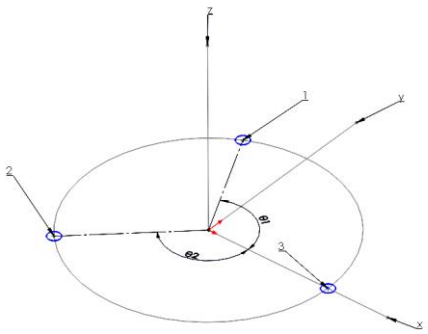

Figure 5. Smiplified schematic. θ_1 and θ_2 are defined as positive angles from the positive x axis, as shown, where the HEMs rotate about radius 'r'.

First, the initial conditions are defined such that the platform is level, where the z height of the center of the platform is such that the attractive force of the HEMs with zero current is equivalent to the total weight and the initial currents are such that are required to maintain the level orientation. Geometrically, we can develop the force transformation:

$$\begin{Bmatrix} F_z \\ T_x \\ T_y \end{Bmatrix} = [T] \begin{Bmatrix} F_1 \\ F_2 \\ F_3 \end{Bmatrix} \quad (2)$$

Where:

$$[T] = \begin{bmatrix} 1 & 1 & 1 \\ r\sin\theta_1 & -r\sin\theta_2 & 0 \\ -r\cos\theta_1 & -r\cos\theta_2 & -r \end{bmatrix} \quad (3)$$

Considering geometric constraints and using a small angle approximation for tipping and tilting, the displacement for each HEM can be given by:

$$\begin{Bmatrix} \delta z_1 \\ \delta z_2 \\ \delta z_3 \end{Bmatrix} = [T]' \begin{Bmatrix} \delta z \\ \delta\alpha \\ \delta\beta \end{Bmatrix} \quad (4)$$

Considering force and moment equilibrium from the initial conditions, the equations of motion can be given as:

$$\begin{Bmatrix} M\ddot{z} \\ I_x\ddot{\alpha} \\ I_y\ddot{\beta} \end{Bmatrix} = \begin{Bmatrix} F_z \\ T_x \\ T_y \end{Bmatrix}_z + \begin{Bmatrix} F_z \\ T_x \\ T_y \end{Bmatrix}_i \quad (5)$$

Where the first and second terms are the force contributions from the z air gaps and HEM currents respectively. This can be expanded as:

$$\begin{Bmatrix} M\ddot{z} \\ I_x\ddot{\alpha} \\ I_y\ddot{\beta} \end{Bmatrix} = k_z TT' \begin{Bmatrix} \delta z \\ \delta\alpha \\ \delta\beta \end{Bmatrix} + \mathrm{k_i} T \begin{Bmatrix} \delta i_1 \\ \delta i_2 \\ \delta i_3 \end{Bmatrix} \quad (6)$$

Where k_i and k_z are the linearized stiffness coefficients. These coefficients differ by HEM and can be found analytically or experimentally. An example distribution is shown in fig. 6 [1].

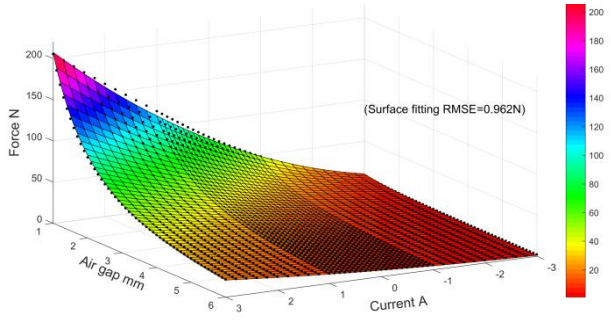

Figure 6. Anylitical and epxeriemental force distribution as a function of airgap and current for a particular HEM [1].

We can then define the state variable:

$$\mathrm{X} = \left[\delta z, \delta\alpha, \delta\beta, \delta\dot{z}, \delta\dot{\alpha}, \delta\dot{\beta}\ \right]' \quad (7)$$

The state space realization becomes:

$$\dot{X} = \begin{bmatrix} 0_{3x3} & I_{3x3} \\ k_z TT' & 0_{3x3} \end{bmatrix} X + \begin{bmatrix} 0_{3x3} \\ k_i T \end{bmatrix} \begin{Bmatrix} \delta i_1 \\ \delta i_2 \\ \delta i_3 \end{Bmatrix} \quad (8)$$

For strictly stability control, this can be expressed as:

$$\dot{X} = AX + B \quad (9)$$

$$Y = CX + DU \quad (10)$$

$$A = \begin{bmatrix} 0_{3x3} & I_{3x3} \\ k_z TT' & 0_{3x3} \end{bmatrix} \quad (11)$$

$$B = \begin{bmatrix} 0_{3x3} \\ k_i T \end{bmatrix} \quad (12)$$

$$C = [I_{3x3}, 0_{3x3}] \quad (13)$$

$$D = [0_{3x3}, 0_{3x3}] \quad (14)$$

The controllability and observability matrices R and Q respectively become:

$$R = [A, AB, A^2B, \ldots A^5B] \quad (15)$$

$$Q = [C, CB, C^2B, \ldots C^5B] \quad (16)$$

Which shows the linearized system is both controllable and observable at all operating points as both matrices R and Q are full rank with non-zero coefficients and where θ_2 is not equal to $-\theta_1$.

E. Control Strategy

While discussing the angular control strategy for θ_1 and θ_2, it is assumed that the stability controller is sufficiently robust so that it can maintain level levitation. The controllability of the system at all operating points has been shown in the previous section, so for a system which moves sufficiently slow with adequate gain scheduling, such a controller is feasible. Robust levitation of magnetically levitated platforms has already been conducted in previous research [1], and is not at focus here currently.

The optimal values for θ_1 and θ_2 for zero-power levitation can be achieved using feedback from the HEM coil currents i_1, i_2, and i_3 during level levitation of the platform.

Since the air gap – and therefor the force contributions – for each HEM's permanent magnet is equal when the platform is level, any variance in the currents i_n is attributed directly to the eccentricity of the load, or in other words to the moment load . For level levitation, when and only when the platform is loaded symmetrically will all currents i_n will be equal. Eccentrically moving the load will then variance in the currents i_n. The moment load about the centroid $T_{C,x}$ and $T_{C,y}$ as a function of i_1, i_2, i_3, and θ_1 and θ_2 is given as:

$$\begin{Bmatrix} T_{C,x} \\ T_{C,y} \end{Bmatrix} = \begin{bmatrix} r\sin\theta_1 - C_y & -r\sin\theta_2 - C_y & -C_y \\ -r\cos\theta_1 - C_x & -r\cos\theta_2 - C_x & -C_x \end{bmatrix} \begin{Bmatrix} i_1 K_i \\ i_2 K_i \\ i_3 K_i \end{Bmatrix} \quad (17)$$

Where K_i is a linearized stiffness coefficient for the operating conditions, and the centroid positions C_x and C_y in x and y respectively are given in eq. (1). As the θ_1 and θ_2 approach

the correct solution, $T_{C,x}$. $T_{C,y}$, and therefore the variance in i_n all approach zero.

Next, we consider the relationship between operating angles θ_1 and θ_2 and eccentric loads, or in other words moment loads. As elaborated in section C, only one solution θ_1 and θ_2 exists for a given eccentric load, which is based on the location of the overall center of mass. The solution exists at the centroid of the thee HEMs and is given by eq. (1).Although the forward solution for x and y of the centroid is straight forward given θ_1 and θ_2, practically, the inverse solution for θ_1 and θ_2 given x and y is computationally taxing. Therefore, for application, it is better to pre-calculate this solution to the resolution of the system's sensors and employ a look-up table for the inverse function. Doing so yields θ_1 and θ_2 as a function of the x and y location of the center of mass. The location of the center of mass correlates to the moment load about the x and y axis as follows:

$$\begin{Bmatrix} T_{0,x} \\ T_{0,y} \end{Bmatrix} = Mg \begin{Bmatrix} C_y \\ -C_x \end{Bmatrix} \tag{18}$$

While the total mass 'M' may be unknown, it can be seen that the direction of moment is not dependent on the total load, only on the location of the centroid.

In summary, the metrics $T_{C,x}$ and $T_{C,y}$ indicate the moment direction of the load, with directional error decreasing as θ_1 and θ_2 approach the correct solution. And, a relationship has been developed which allows the control of moment loads in x in y through adjustments of θ_1 and θ_2. Together, using θ_1 and θ_2 to adjust the zero power moment of the centroid in x and y based on moment in the direction indicated by $T_{C,x}$ and $T_{C,y}$, with sufficiently small steps or a sufficiently slow trajectory, convergence to the zero power solution for θ_1 and θ_2 can be archived independently to the z height zero power solution.

F. Numerical Example

A numerical example is provided to verify the convergence of the control strategy. Again, the solution is expected to converge as the calculated moment about the HEM's calculated centroid becomes a closer to a pure moment as the HEM centroid approaches the location of the center of mass.

Let the arbitrary initial conditions of the simulation be given as in table 1:

TABLE I. INITIAL CONDITIONS FOR NUMERIC SIMULATION

Variable	Parameter	Value
r	Radius to HEM	1 (m)
Cx	Center of Mass x	-0.19(m)
Cy	Center of Mass y	0.19 (m)
K_i	Current Stiffness	1 (N/A)
$\theta_{1,0}$	Initial Angle HEM 1	$2\pi/3(rad)$
$\theta_{2,0}$	Initial Angle HEM 2	$2\pi/3\ (rad)$
Fz	Force Contribution Air Gap	0.5Mg (N)
dx	Maximum Step Size	0.025 (m)

Fig. 7 shows a simplified block diagram for the numerical analysis.

It is important to note that the weight of the load is only partially accommodated by the z height of the platform. This is the most generic case of the solution, and shows that the angular solution can be found for zero power independently from the z solution.

A simplified block diagram, shown in fig. 7, outlines the overall method of the iterative calculation. Again, it is assumed that the system can remain level at all times. Firstly, the current at each HEM is calculated by solving the system of equations, where $i_1 = F_i$ due to a stiffness of 1.

$$\begin{Bmatrix} Mg \\ C_y Mg \\ C_x Mg \end{Bmatrix} = [T] \begin{Bmatrix} i_1 \\ i_2 \\ i_3 \end{Bmatrix} \tag{17}$$

Next, eq. (17) is used to calculate the moment about the centroid of the HEMs in x and y. The centroid of the HEMs is then moved proportionally to the moment about the centroid. Positive motions of the centroid along the x and y

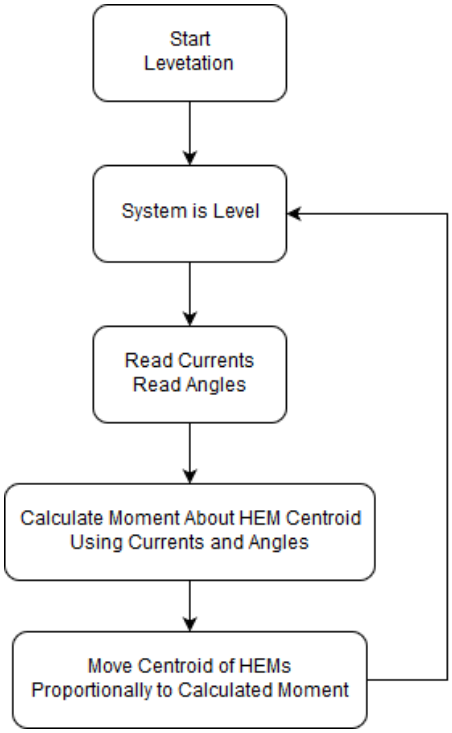

Figire 7. Block diagram showing loop for iterative numerical simulation.

axes correspond with increasing moment around y and negative moment about x respectively. The centroid is moved in sufficiently small steps to prevent overshoot of the solution. The centroid position then uniquely corresponds to angle pair θ_1 and θ_2 which can be solved from the inverse of eq. (1). Again, as this task is computationally taxing, the inverse mapping is best pre-calculated for operation. Finally, using the new HEM angular positions, the current is recalculated, and the loop reiterated until convergence.

The simulation results for the conditions in table 1 are presented in fig. 8. It can be seen by the blue line that variance converges by 40 iterations. Here, variance has been scaled by 1000 for ease of viewing. The centroid position of the HEMs can be seen to converge to location of the center of mass. Finally, it can see the angular positions θ_1 and θ_2 converge to 2.2106 and 2.9068 radians, respectively.

Again, it should be stressed that the overall system at this point is not in a the absolute zero power state, as the its z height only allows for 0.5Mg to be passively accommodated. Convergence of current variance to zero only indicates that the currents through the coils are equal; not necessarily that they are zero. However, as mentioned before, the zero power values for θ_1 and θ_2 are independent from the zero power z height. In other words, the discovered zero power θ_1 and θ_2 for this load is valid all z heights, including the zero power z height.

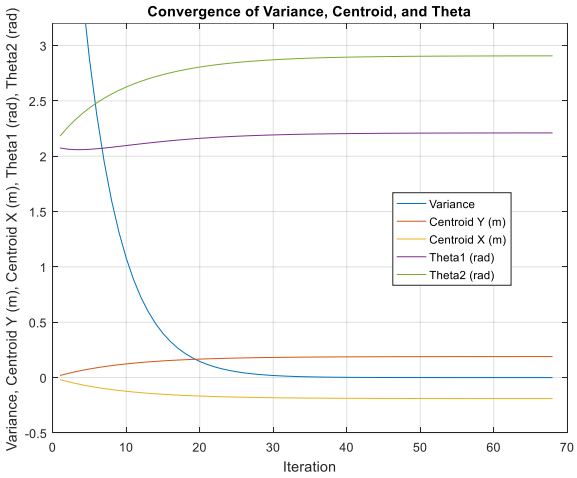

Figire 8. Simulation results. HEM Centroid position converges to {-0.19,0.19} (m), Variance converges to zero, and theta 1 and theta two converge to 2.2106 2.9068 (rad) respectively.

With this in mind, considering a zero power z height controller has already been developed in the past [1] it is feasible to say that with a closed loop system employing the described control strategy for zero power θ_1 and θ_2 , combined with a zero power z controller, orientation controlled zero power of a level platform can be achieved.

G. Conclusion

The novel system for orientation controlled zero power levitation was proposed. The controllability and observability of the system was verified at all operating points. The operating space of the system was determined, and an engineering operating space was selected. A control strategy was introduced for the HEM angles, and was numerically verified to converge to the zero power angular solution. Combined with past work on a zero power z controller, the feasibility of the novel system was established.

Further, it was established that the zero power angular solution is independent from the zero power z solution. This aspect of operation makes the system particularly applicable for repeated pick and place operations where the center of mass is similarly located for each cycle. In such a case, initial the HEM angles would be calibrated by statically suspending the object. Then, for subsequent cycles, the control currents would have lower variance due to a lower eccentricity of the center of mass from the centroid, thus reducing power consumption.

REFERENCES

[1] B. Annasiwaththa, H. Akinori, and O. Koichi, "Design concept and analysis of a magnetically levitated linear slider with non-contact power transfer." International Journal of Applied Electromagnetics and Mechanics, pp. 52.1-2, 2016

[2] J. Lin, A. Harada and K. Oka, "Arbitrarily close equilibrium orientaitons of magnetically levitated platforms," 2017 11th International Symposium on Linear Drives for Industry Applications (LDIA), Osaka, 2017, pp. 1-4.